








Fusion and proton transfer in the $^{10}\text{B} + ^{27}\text{Al}$ system at sub-barrier energies

V. R. Sharma ^{1,*} E. F. Aguilera ^{2,†} T. L. Belyaeva ³ J. C. Morales-Rivera ^{2,3} P. Amador-Valenzuela ²
E. Martínez-Quiroz ² L. Acosta ¹ and D. Lizcano⁴

¹*Instituto de Física, Universidad Nacional Autónoma de México, Apartado Postal 20-364, 01000 México City, México*

²*Departamento de Acelerador y Estudio de Materiales, Instituto Nacional de Investigaciones Nucleares, Apartado Postal 18-1027, 11801, México, D.F., México*

³*Facultad de Ciencias, Universidad Autónoma del Estado de México, 50000 Toluca, México*

⁴*Departamento de Desechos Radiactivos, Instituto Nacional de Investigaciones Nucleares, 11801 México City, México*



(Received 16 June 2021; accepted 7 October 2021; published 29 October 2021)

Background: Significant enhancement in sub-barrier fusion cross sections by several orders of magnitude, in the frame of one-dimensional barrier penetration models, is observed for a variety of nuclear systems. To understand this, one needs to find the fundamental degrees of freedom relevant in the sub-barrier fusion region by incorporating nonelastic channels such as coupling of the excited target and/or projectile nuclei, particle transfer channels, threshold variation of nuclear potential, etc.

Purpose: We probe what degrees of freedoms are associated with the $^{10}\text{B} + ^{27}\text{Al}$ reaction at energies $\approx 18\%$ below to $\approx 12\%$ above the Coulomb barrier.

Method: An online γ -ray spectroscopy technique is used to determine the populated excitation functions in the $^{10}\text{B} + ^{27}\text{Al}$ reaction. The reaction cross sections obtained from these γ rays are compared with the statistical model to explore the mechanism of fusion reactions.

Results: At energies near and below the Coulomb barrier, two isotopes of sulfur (^{34}S and ^{32}S) were found to reproduce cross section within the frame of the PACE2 model based on Hauser-Feshbach calculations, whereas isotopes of chlorine (^{35}Cl), sulfur (^{35}S), and phosphorous (^{32}P) agree well but at above-barrier energies. Isotopes of Ar, Cl, S, P, and Si show significant enhancement over an entire band of energies. This enhancement (suppression) in the experimental cross section at energies above (below) the barrier points towards the involvement of some nuclear reaction mechanism other than fusion-evaporation. Distorted-wave Born approximation calculations strongly support the population of ^{28}Si residue via the one-proton transfer process. The total fusion cross section is found to follow the theory after the inclusion of coupling of low lying excited states of projectile and target. Calculations concerning the astrophysical S factor and the logarithmic derivative factor support the idea of no fusion hindrance at the studied energies. The universal fusion function benchmark shows consistency with previous data for lithium (or Li isotopes) induced systems.

Conclusions: The inclusion of inelastic couplings associated with both target and projectile is important to understand the behavior of total fusion cross section. The formation of ^{28}Si via the one-proton transfer reaction supports the present experimental technique to make inclusive transfer measurements. The calculations with the universal fusion function present a slight suppression in the higher energy region, indicating possible breakup effects in this region. The present calculations show that till 18% below the barrier there is no fusion hindrance. On extrapolating the theoretical values we further observed that the present system has no fusion hindrance. No connection of $^{10}\text{B} + ^{27}\text{Al}$ fusion with astrophysics has been made, which raises the question to think of cosmic ray reactions and perhaps reactions in the early solar system, but how the fusion reaction would fit into the picture is not clear at all.

DOI: [10.1103/PhysRevC.104.044621](https://doi.org/10.1103/PhysRevC.104.044621)

I. INTRODUCTION

The near- and sub-barrier fusion processes in reactions induced by weakly bound projectiles have attracted much attention in recent years and have been the subject of many studies, both experimental and theoretical [1–6]. In this re-

gard, a correct description of the elastic scattering cross sections becomes a priority goal. Thus, the proper reaction mechanism and an adequate choice of optical potentials play an important role. The respective theoretical analysis of reactions involving weakly bound projectiles can be more challenging if the effect of couplings to nonelastic channels is sufficiently strong. For example, dynamics of some reactions induced by weakly bound or radioactive nuclei can be affected by coupling to the projectile breakup mechanism due to the low breakup threshold energy [7–11]. Experimentally,

*vijayraj@fisica.unam.mx

†eli.aguilera@inin.gob.mx

the influence of breakup on the fusion cross section leads to fusion suppression or enhancement at energies, respectively, above or below the Coulomb barrier, in comparison with the results obtained from calculations within the one-dimensional barrier penetration model (1DBPM) [12–15]. In Refs. [16–20] it was shown that the observed fusion suppression at above-barrier energies might be attributed to the incomplete fusion (ICF) process, and the magnitude of the suppression is a function of the breakup threshold energy of the projectile [19]. On the other hand, classification of ICF over complete fusion processes for stable projectiles on heavy targets was attempted by our group on the basis of spin distribution measurements [21–23]. Recently, Lee and Diaz-Torres [24] calculated the effectiveness of population of higher spin states of a compound nucleus due to the ICF process at energies near and above the Coulomb barrier in the frame of a classical dynamic reaction model. It was shown that the evaporation of the charged particles from a compound nucleus for the heavier systems is hindered due to the higher Coulomb barrier, because both the repulsive Coulomb and the centrifugal forces dominate over the attractive nuclear field. This opens the door to fusion suppression above the barrier height via breakup processes.

Indeed, a convenient way to investigate the effects of breakup on fusion cross sections is to study the corresponding suppression factors above the barrier. A systematic of such suppression factors for heavy targets indicates that, for a given projectile, they seem to depend only weakly on the target mass [25]. For lighter targets, however, one would expect Coulomb breakup to be relatively less important, which could possibly change the above results. In an attempt to estimate the effect of breakup of the projectile on the fusion reaction involving lower mass targets, Kumawat *et al.* [26] proposed the existence of a universal suppression factor of approximately 30% for over-the-barrier complete fusion (CF) of a weakly bound projectile with different targets. Beck *et al.* [27] reported that the suppression factor is not unique at above barrier energies and is approximately 15% of CF cross section for the lighter or medium mass systems, if one considers ${}^6\text{Li} + {}^{59}\text{Co}$.

To understand fusion phenomena below the Coulomb barrier, a very limited number of studies are available with medium mass targets. In this regard, DiPietro *et al.* [28] in their pioneering experiment reported that the enhancement of total reaction cross section at sub-barrier energies is due to the contributions from ICF process or single-particle transfer reaction processes. However, Jia *et al.* [29] suggested that positive Q -value neutron transfer is a more favorable step for fusion cross section enhancement in the sub-barrier region. Sargsyan *et al.* [30] found that the enhancement in the sub-barrier energy region due to particle transfer is not because of Q values for the transfer channels but it appears because of the change in structure of the resultant nuclei after inelastic collisions and neutron transfer. The studies of Kohley *et al.* [31], Jacob *et al.* [32], and Lin *et al.* [33] do not concur that fusion cross section enhancement is because of single-particle (neutron) transfer reactions at sub-barrier energies. Lighter systems concerning ${}^6\text{Li}$ and ${}^7\text{Li}$ projectiles with ${}^{24}\text{Mg}$ target [34] reportedly follow quite well the respective fusion

cross sections obtained from the 1DBPM calculations at energies around the barrier indicating that no breakup process is involved despite the fact that both projectiles are loosely bound nuclei.

Owing to the low breakup threshold energy, among the most studied stable weakly bound nuclei are ${}^6\text{Li}$, ${}^7\text{Li}$, and ${}^9\text{Be}$, but no studies are available with the ${}^{10}\text{B}$ nucleus with light or medium mass targets at below-barrier energies. Peering its structure with stable nuclei provides information that ${}^{10}\text{B}$ has low α separation energy of 4.46 MeV, which can lead to breakup leaving a ${}^6\text{Li}$ residual nucleus. This characteristic, common with weakly bound nuclei, makes it an ideal nucleus for exhaustively studying the influence of the breakup process and its effects on total reaction cross sections at energies around the barrier. Note that a systematic fusion excitation function measurement carried out by Aversa *et al.* [35] for ${}^{10}\text{B}$ nuclei with a ${}^{197}\text{Au}$ target explains the importance of couplings of the one-neutron transfer channel to describe the fusion data in the sub-barrier energy region.

In the context of discussed results, it is worthwhile to measure the fusion cross section for a system with ${}^{10}\text{B}$ projectile on low mass targets. The present work deals with the measurements of excitation functions (EFs) for the ${}^{10}\text{B} + {}^{27}\text{Al}$ system at energies $\approx 18\%$ ($\approx 12\%$) below (above) the Coulomb barrier, respectively. To the best of our knowledge, the EFs for this system at the proposed energies have been measured here for the first time. Note that the energies measured in the present work are smaller than those described in Refs. [34,36–41], therefore, no fusion suppression is expected in the present data. Presentations of the data in the frame of the statistical model, distorted wave Born approximation (DWBA) calculations, and coupled channel calculations are performed to understand the nature of the enhancement or suppression in the total fusion cross sections, if any. An attempt is made to understand the behavior of total fusion by comparing with other lighter systems using the universal fusion function (UFF) reduction procedure [35]. The paper is organized as follows. The experimental procedure and data reduction method are given in Sec. II. The results of the experiment and respective interpretation in the frame of theoretical models are presented in Sec. III. Deduction of the astrophysical S factor, the logarithmic derivative factor and comparison of experimental data with available literature values are presented in corresponding subsections of Sec. III, while Sec. IV summarizes the findings of the present work.

II. EXPERIMENTAL PROCEDURE AND DATA REDUCTION

The experiment was performed using a ${}^{10}\text{B}^{5+}$ beam from the 6 MV Tandem accelerator located in the state of México at Instituto Nacional de Investigaciones Nucleares, México. A single self-supporting target of isotopically pure (99.9%) aluminum (${}^{27}\text{Al}$) was used, of thickness ≈ 1.71 mg/cm² which was measured by the α -transmission method. Further, the target foil was cut into 1.2×1.2 cm² size and pasted on a stainless steel target ladder having a concentric hole of 1.0 cm diameter. The irradiation was performed in a scattering chamber of 25 cm diameter at beam energies

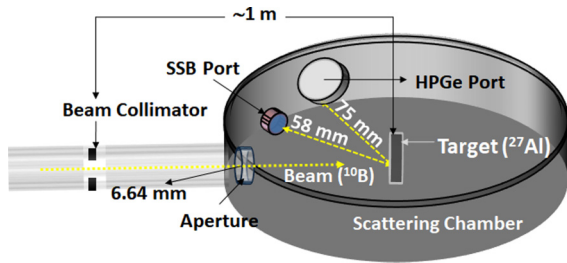


FIG. 1. A scheme of the experimental setup; see text for details.

≈ 1.2 – 1.7 MeV/nucleon with almost constant beam current ≈ 40 – 50 nA. A high-purity germanium (HPGe) detector was placed at 125° with respect to the beam direction, an angle that effectively minimizes possible effects of anisotropies in the emitted γ rays [42,43]. The detector resolutions were 2.0–2.6 keV for 121–1408 keV γ -ray lines measured from a standard ^{152}Eu radioactive source. Notwithstanding, data for absolute efficiency were taken by placing calibrated radioactive sources of ^{241}Am , ^{152}Eu , ^{137}Cs , ^{133}Ba , and ^{60}Co at the target position before and after the experiment. A silicon surface barrier (SSB) detector was positioned at 150° with respect to the beam axis and was calibrated with a triple α source (^{239}Pu / ^{241}Am / ^{244}Cm). The positions of the detectors along with ancillary components of the experimental setup are shown in Fig. 1.

The ^{10}B beam entered the scattering chamber passing through a collimator of 6.64 mm diameter, which is the only aperture present in the scattering chamber. The beam size is defined by beam collimation slits placed at approximately 1 m distance from the target position. The characteristic γ lines produced during the reaction were recorded online by a HPGe detector with a target to detector distance ≈ 75 mm. Measure-

ments of Rutherford scattering of the beam were recorded by a SSB detector placed at ≈ 58 mm from the target to determine the absolute normalization factors for the specific equipment alignment or beam focusing conditions. Both detectors were coupled to the fast multi-parameter data acquisition system GAMMA. Additionally, spectra with beam on a Ta frame having a hole in the place of target were also recorded as well as beam-off background spectra to identify the possible impurity or mixing lines present in the measured γ -ray spectra. No significant contribution of reactions, with the target frame or from background radiation, was thereby found to the relevant γ -ray lines corresponding to the evaporation residue yields.

A typical γ -ray spectrum obtained with beam on the target at the highest projectile energy is shown in Fig. 2. In this figure, the γ peaks corresponding to all identified reaction residues in the present work are assigned. Further, the fusion-evaporation cross sections were obtained from these γ -ray peaks for the identified residues using standard relations as described in Ref. [42] and are tabulated in Table I together with statistical errors (SE).

Note that the systematic errors may also reflect the quality of cross sectional measurements, therefore critical evaluations of uncertainties in various quantities were incorporated. Some of the factors which may introduce systematic errors are

- (i) Nonuniformity of the sample foil may lead to an uncertainty in the determination of the number of target nuclei in the sample. It is hard to know the uncertainty in the target thickness of the rolled foil; however, to check the uniformity of the sample foil, the thicknesses of the samples were measured at different locations of the same sample by the α -transmission method. It is estimated that the error in the target thickness is $\leq 1\%$.

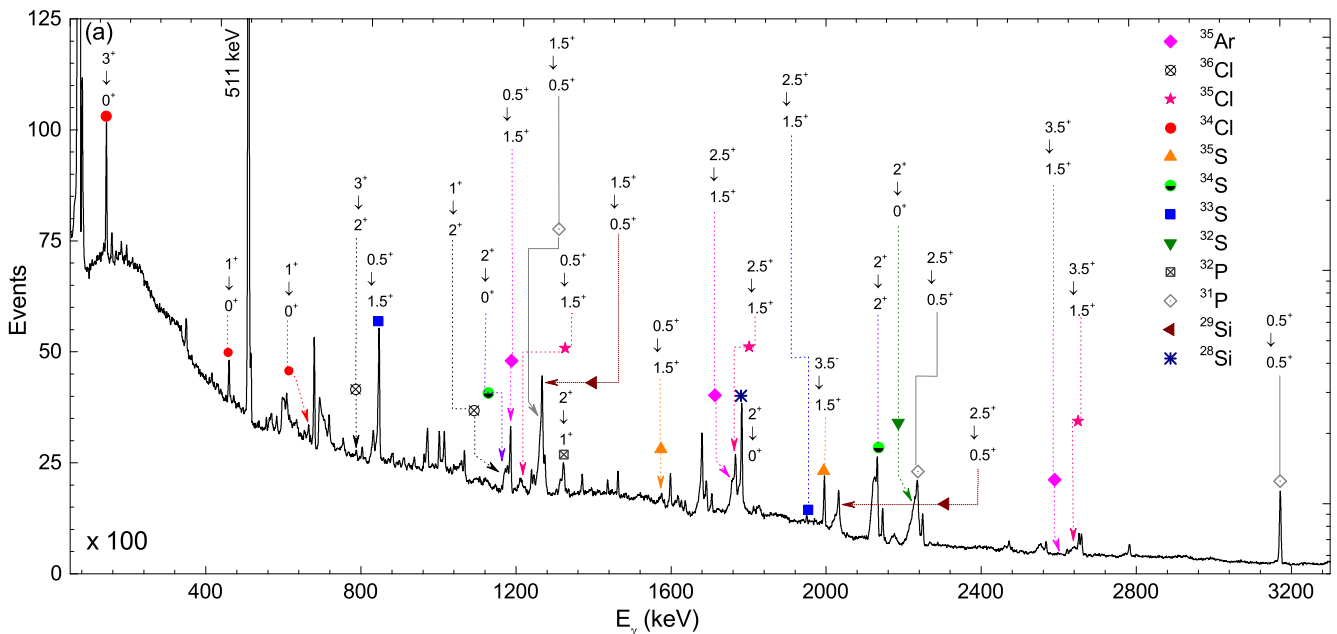


FIG. 2. Typical γ -ray spectrum with beam on target at projectile energy ≈ 15.7 MeV. γ peaks indicate all identified reaction residues in the present work. The initial and final spin-parity of the states involved in the corresponding γ -ray transition also are shown.

TABLE I. Experimentally measured production cross sections (mb) \pm SE for identified residues in the present work.

E_{Lab}^w (MeV)	^{35}Ar	^{36}Cl	^{35}Cl	^{34}Cl	^{35}S	^{34}S	^{33}S
15.7	2.21 \pm 0.04	2.23 \pm 0.10	53.93 \pm 0.90	6.09 \pm 0.11	19.43 \pm 0.18	9.86 \pm 0.12	29.08 \pm 0.82
15.3	1.88 \pm 0.04	2.05 \pm 0.10	41.83 \pm 0.77	4.21 \pm 0.09	14.07 \pm 0.15	8.34 \pm 0.11	24.72 \pm 0.73
15.0	1.69 \pm 0.04	1.92 \pm 0.10	37.87 \pm 0.78	3.93 \pm 0.09	14.12 \pm 0.16	7.24 \pm 0.11	32.03 \pm 0.87
14.6	1.09 \pm 0.03	1.89 \pm 0.08	30.92 \pm 0.58	2.51 \pm 0.06	11.20 \pm 0.11	5.78 \pm 0.08	18.03 \pm 0.49
14.2	0.96 \pm 0.02	1.49 \pm 0.06	25.01 \pm 0.40	1.92 \pm 0.04	7.60 \pm 0.08	4.12 \pm 0.06	12.99 \pm 0.34
13.8	0.84 \pm 0.03	1.34 \pm 0.07	18.25 \pm 0.44	1.03 \pm 0.04	5.59 \pm 0.08	2.81 \pm 0.06	15.47 \pm 0.48
13.4	0.78 \pm 0.02	0.85 \pm 0.05	13.83 \pm 0.31	0.91 \pm 0.03	4.03 \pm 0.06	1.65 \pm 0.04	8.78 \pm 0.26
12.9	0.52 \pm 0.02	1.04 \pm 0.05	12.63 \pm 0.25	0.29 \pm 0.01	2.13 \pm 0.04	0.70 \pm 0.02	3.62 \pm 0.17
12.5	0.44 \pm 0.01	0.42 \pm 0.02	5.14 \pm 0.09	0.20 \pm 0.01	0.93 \pm 0.01	0.16 \pm 0.01	1.97 \pm 0.04
12.0	0.30 \pm 0.01	0.30 \pm 0.03	2.10 \pm 0.11	0.12 \pm 0.01	0.33 \pm 0.02	0.08 \pm 0.003	0.47 \pm 0.14
11.6	0.05 \pm 0.002	0.23 \pm 0.02	1.09 \pm 0.07	0.08 \pm 0.01	0.15 \pm 0.01	0.02 \pm 0.001	0.35 \pm 0.05
E_{Lab}^w (MeV)	^{32}S	^{32}P	^{31}P	^{29}Si	^{28}Si	$\sigma_{TM}^{\text{Exp a}}$	$\sigma_{\text{TF}}^{\text{Exp b}}$
15.7	14.85 \pm 0.14	41.78 \pm 0.16	65.33 \pm 0.86	34.97 \pm 0.61	9.99 \pm 0.11	290.05 \pm 1.7	280.24 \pm 1.6
15.3	12.76 \pm 0.13	37.29 \pm 0.16	45.96 \pm 0.64	30.11 \pm 0.56	8.64 \pm 0.10	231.99 \pm 1.4	225.68 \pm 1.4
15.0	10.07 \pm 0.12	28.17 \pm 0.13	32.53 \pm 0.55	25.12 \pm 0.53	7.84 \pm 0.10	202.58 \pm 1.4	197.14 \pm 1.4
14.6	7.93 \pm 0.09	23.44 \pm 0.10	24.05 \pm 0.41	21.00 \pm 0.41	6.63 \pm 0.08	154.52 \pm 1.0	149.31 \pm 1.0
14.2	5.39 \pm 0.06	17.12 \pm 0.07	16.72 \pm 0.27	16.12 \pm 0.29	5.48 \pm 0.06	114.94 \pm 0.7	110.41 \pm 0.7
13.8	4.33 \pm 0.07	11.23 \pm 0.06	8.90 \pm 0.26	9.27 \pm 0.27	4.37 \pm 0.06	83.46 \pm 0.8	79.28 \pm 0.8
13.4	2.92 \pm 0.04	7.16 \pm 0.04	5.81 \pm 0.15	6.54 \pm 0.19	3.39 \pm 0.04	56.66 \pm 0.5	53.40 \pm 0.5
12.9	1.47 \pm 0.03	3.88 \pm 0.03	3.07 \pm 0.11	3.37 \pm 0.11	2.06 \pm 0.03	34.80 \pm 0.4	32.51 \pm 0.4
12.5	0.44 \pm 0.01	1.62 \pm 0.01	0.77 \pm 0.02	1.56 \pm 0.05	1.08 \pm 0.01	14.75 \pm 0.1	13.43 \pm 0.1
12.0	0.30 \pm 0.01	0.94 \pm 0.01	0.41 \pm 0.05	0.52 \pm 0.06	1.06 \pm 0.01	6.95 \pm 0.2	5.72 \pm 0.2
11.6	0.13 \pm 0.004	0.38 \pm 0.01	0.07 \pm 0.01	0.30 \pm 0.03	0.56 \pm 0.01	3.43 \pm 0.1	2.90 \pm 0.1

^a σ_{TM}^{Exp} = total measured cross section.

^b $\sigma_{\text{TF}}^{\text{Exp}}$ = $\sigma_{TM}^{\text{Exp}} - \sigma(^{28}\text{Si})$. See text for details.

- (ii) During the irradiations, the beam current may fluctuate, which may result in the variation of the number of incident particles during the bombardment. Simulations from the SIMNRA software were performed to check the number of projectiles, and it was estimated that this source may introduce an error of not more than 5% in the measured cross sections.
- (iii) Uncertainty in the determination of the geometry-dependent efficiency of the γ -ray spectrometer may introduce additional error in the measured cross sections. The efficiency of the HPGe detector was measured before and very frequently during the run, using calibrated sources of ^{60}Co , ^{133}Ba , ^{137}Cs , and ^{152}Eu . Statistical errors in counting of the standard sources may also introduce errors in the efficiency, which were minimized by accumulating a large number of counts for comparatively long times (≈ 4000 s). Experimental data on the geometry-dependent efficiencies with γ -ray energy at a fixed source-detector separation has been fitted with a power law curve. The uncertainty due to the fitting of the efficiency curve is estimated to be 5%. In the present work, the overall systematic error excluding the uncertainty in branching ratio, decay constant, etc., which have been taken from the *Table of Radioactive Isotopes* [44] is estimated to be $\leq 7\%$.

For the representation of the data (E_n, σ_n), the energy loss in the target was accounted for by considering an analytical

function $f_1(E)$ fitting the data, that provides a new energy for the n th point as the weighted average energy E^w [45]:

$$E_n^w = \frac{\int_{E_n}^{E_n^f} E f_1(E) dE}{\int_{E_n}^{E_n^f} f_1(E) dE}, \quad (1)$$

where E_n^f is the projectile energy after traversing the target. The new data points (E_n^w, σ_n) produce a second function $f_2(E)$ which, when used instead of $f_1(E)$ in Eq. (1), produces in turn a new set of energies. This iterative process is repeated until self-consistent results are obtained.

The energy loss at target varied from 5.2 to 5.9 MeV, corresponding to the highest and lowest beam energies, respectively. The beam energy is precise to 0.15% (about ± 20 keV) but, after applying Eq. (1), an uncertainty of ± 35 keV is estimated on the final reported energy, based on the differences obtained for the energies in the last iterations of Eq. (1).

III. ANALYSIS OF THE DATA AND INTERPRETATION OF RESULTS

The experimental cross sections of the studied reactions are presented in Table I for the residual isotopes of Ar, Cl, S, P, and Si, to be compared with the statistical model predictions in order to understand the involved degrees of freedom. First of all, we analyze the data using the PACE2 code [46]. Afterwards, the DWBA calculations are done to understand

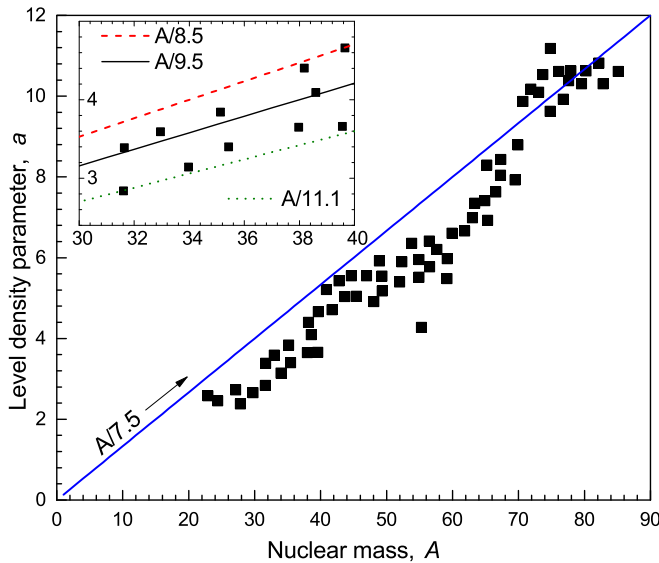


FIG. 3. Values of the level density parameter a , obtained from the analysis as suggested by [48]. The straight line corresponds to $a = A/7.5$. A zoom in the nuclear mass region $30 < A < 40$ is shown in the inset where $a = A/9.5$ approximates the average trend in this region, with upper (lower) limit given by $a = A/8.5$ ($a = A/11.1$).

the possibility of a proton transfer from the projectile to the target nucleus. Later, the experimental total fusion cross sections ($\sigma_{\text{TF}}^{\text{Exp}}$) are compared with calculations carried out within the 1DBPM and the coupled channel calculations. In addition, the astrophysical S factor and the logarithmic derivative $L(E_{\text{c.m.}})$ factor are deduced from the $\sigma_{\text{TF}}^{\text{Exp}}$ to investigate the phenomenon of fusion hindrance. Finally, we present some estimates to generate a systematics in the frame of the UFF.

A. Analysis with evaporation code PACE2

We analyze the production cross sections of evaporation residues within the Hauser-Feshbach mechanism of the compound nucleus (CN) formation model using the computer code PACE2 [46]. It is important to mention that we used the updated version of the original code PACE2 by incorporating the AME12 mass table [47] and corrections of the neutron optical model potential parameters, as explained in our previous work [1]. As suggested by the author of the code PACE2 [46], the yrast line was determined by the liquid drop rotational energy and the Sierk fission barrier was assumed throughout the calculations. But the regular Wapstra mass table supplied with the code was replaced by the AME12 table for all involved nuclei.

Since the level density parameter is one of the crucial ingredients of any statistical model calculation, an attempt has been made to deduce the values of a from the analysis of nuclear mass A as suggested in Ref. [48]. In Fig. 3, the level density parameter curve is plotted with nuclear mass $A < 90$, where $a = A/7.5$ corresponds to the default value used in code PACE2. As can be seen in the figure, the CN corresponding to the $^{10}\text{B} + ^{27}\text{Al}$ system is $^{37}\text{Ar}^*$, which is below the group of nuclei described by the default value of a ; therefore, suitable

values of a were obtained by fitting the nuclear masses. In the inset of Fig. 3 a zoom in of the region $30 < A < 40$ shows the upper (lower) limits of $a = A/8.5$ ($a = A/11.1$), with an approximate $a = A/9.5$ the average trend in this region.

The predictions of PACE2 at new values of a and considering the experimental fusion cross section as an input of code PACE2 were then used to compare with the measured fusion cross sections for identified evaporation residues, viz., $^{35}\text{Ar}(2n)$, $^{36}\text{Cl}(p)$, $^{35}\text{Cl}(pn)$, $^{34}\text{Cl}(p2n)$, $^{35}\text{S}(2p)$, $^{34}\text{S}(2pn)$, $^{33}\text{S}(\alpha)$, $^{32}\text{S}(\alpha n)$, $^{32}\text{P}(\alpha p)$, $^{31}\text{P}(\alpha pn)$, $^{29}\text{Si}(2\alpha)$, and $^{28}\text{Si}(2\alpha n)$. The inclusion of the experimental total fusion cross section in code PACE2 is an iterative way to deduce the theoretical cross section, which means that the code internally shifts the respective optical model transmission coefficients to reproduce cross sectional values.

Figures 4(a)–4(l) show the experimentally measured EFs in frame of PACE2 predictions. As can be seen in Figs. 4(a), 4(f), and 4(h) the experimental cross section for evaporation residues (ERs) $^{35}\text{Ar}(2n)$, $^{34}\text{S}(2pn)$, and $^{32}\text{S}(\alpha n)$ are suppressed at above-barrier energies, indicating a possible involvement of another dominating mechanism. On the other hand, at energies near and below the barrier the experimental cross section for ERs $^{34}\text{S}(2pn)$ and $^{32}\text{S}(\alpha n)$ are well reproduced by PACE2 predictions, indicating their production via CF mode. At barrier energies, the ER $^{35}\text{Ar}(2n)$ starts to follow the statistical predictions, but at sub-barrier energies the experimental cross section is enhanced and points towards a possible involvement of another reaction channel. Similar behavior at below-barrier energies has been observed [see Figs. 4(c), 4(e), and 4(i)] for the EFs $^{35}\text{Cl}(pn)$, $^{35}\text{S}(2p)$, and $^{32}\text{P}(\alpha p)$; however, at energies near and above the barrier the experimental cross section is found to be well reproduced by statistical model predictions, which indicates its production through the complete fusion mode only. In the cases of $^{36}\text{Cl}(p)$, $^{34}\text{Cl}(p2n)$, $^{33}\text{S}(\alpha)$, $^{31}\text{P}(\alpha pn)$, $^{29}\text{Si}(2\alpha)$, and $^{28}\text{Si}(2\alpha n)$, the experimental cross sections [see Figs. 4(b), 4(d), 4(g), 4(j), 4(k), and 4(l)] are found to be substantially higher than PACE2 predictions at the entire studied energy region.

The evident disagreement of PACE2 calculations with some of the measured EFs of Fig. 4 (e.g., ^{36}Cl , ^{35}Cl , ^{33}S , ^{31}P , and ^{29}Si) indicates that some other mechanism, different from CF followed by particle evaporation, is contributing to the data. A possible hypothesis is that the incomplete fusion (ICF) mechanism, which would not be accounted for in PACE2, is probably the main contributor. A few possibilities can be mentioned here to support this hypothesis. The low separation energy of ^{10}B into $^6\text{Li} + \alpha$ ($S = 4.46$ MeV) could favor ICF with ^6Li , through the process $^{10}\text{B} + ^{27}\text{Al} \rightarrow ^6\text{Li} + \alpha + ^{27}\text{Al} \rightarrow ^{33}\text{S} + \alpha$, which could explain the discrepancy seen for ^{33}S . Exclusive measurements of α and ^6Li ejectiles in the $^{10}\text{B} + ^{27}\text{Al}$ reaction [49] at energies above the barrier indicated the presence of ICF and direct cluster transfer (DCT) processes. ICF can be thought of as a sequential process where the projectile is first split into two clusters ($^{10}\text{B} \rightarrow ^6\text{Li} + \alpha$) and then one of the clusters fuses with the target. DCT, on the other hand, refers to a direct transfer of one of the clusters from the projectile to the target. Both these processes could contribute to increase the ^{33}S yield when the absorbed cluster is ^6Li ,

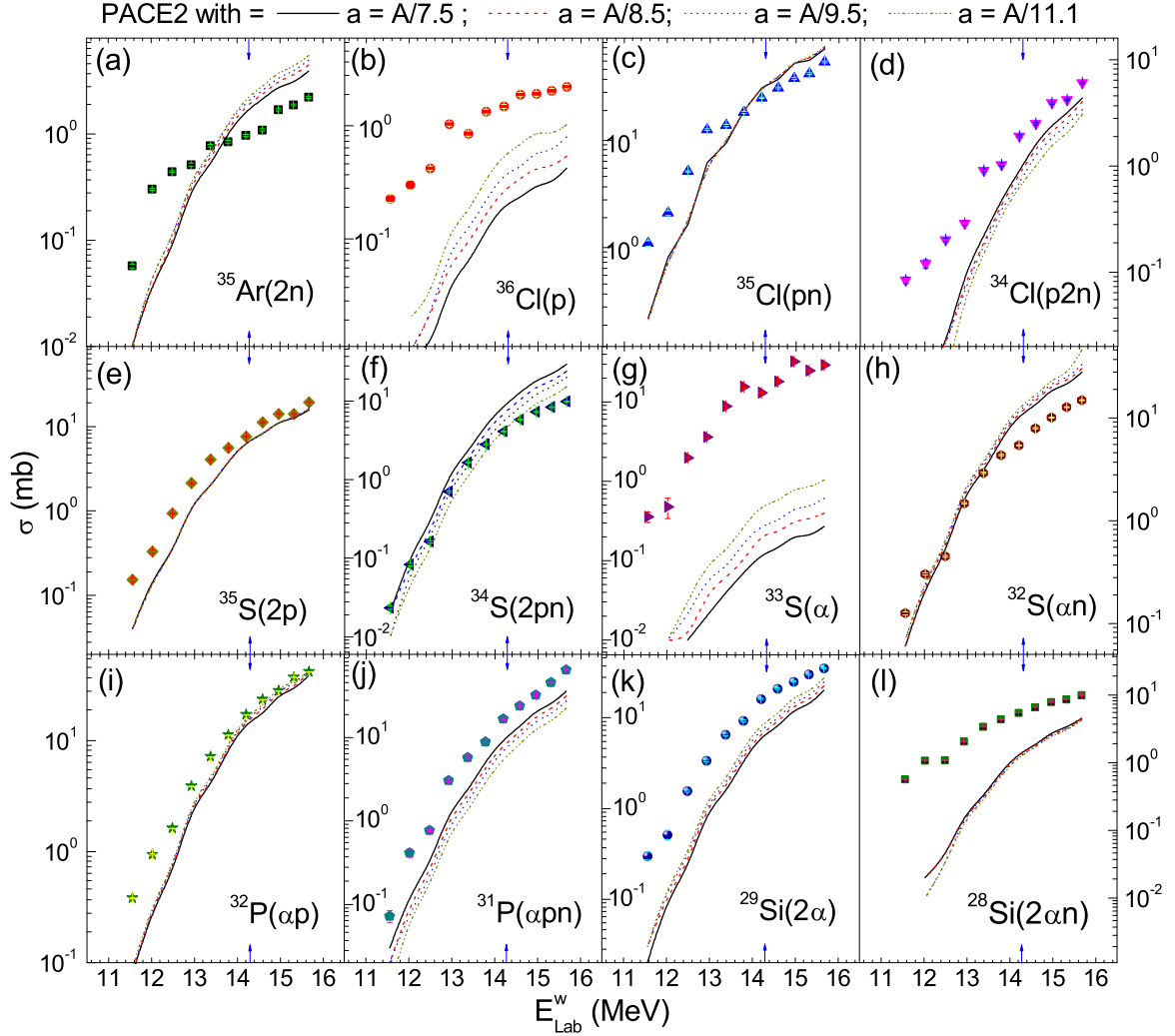


FIG. 4. Experimentally measured cross section \pm SE of evaporation residues (a) $^{35}\text{Ar}(2n)$, (b) $^{36}\text{Cl}(p)$, (c) $^{35}\text{Cl}(pn)$, (d) $^{34}\text{Cl}(p2n)$, (e) $^{35}\text{S}(2p)$, (f) $^{34}\text{S}(2pn)$, (g) $^{33}\text{S}(\alpha)$, (h) $^{32}\text{S}(\alpha n)$, (i) $^{32}\text{P}(\alpha p)$, (j) $^{31}\text{P}(\alpha pn)$, (k) $^{29}\text{Si}(2\alpha)$, and (l) $^{28}\text{Si}(2\alpha n)$ are compared with PACE2 predictions with different a values. See the text for an explanation.

which would explain the observed enhanced data. Likewise, if in the above process ICF occurs instead with the α particle of the intermediate stage, a ^{31}P nucleus would be formed, which could in turn explain the respective disagreement seen in this later residue. ^{10}B can also be separated into $^8\text{Be} + d$ ($S = 6.03$ MeV), which could favor ICF with d , producing part of the ^{29}Si observed in Fig. 4(k). On the other hand, ICF with the corresponding ^8Be cluster could in turn explain the discrepancy seen for ^{35}Cl . The ^{36}Cl residue, with a maximum cross section of 2.2 mb, is not too relevant for the total yield, but the respective discrepancy with PACE2 calculations could be due to ICF with a ^9Be cluster. The separation energy of ^{10}B into $^9\text{Be} + p$ is $S = 6.59$ MeV, a value still lower than average. It is worth mentioning that in the case of a $^7\text{Be} + ^{28}\text{Si}$ experiment at near barrier energies [50], with a projectile cluster structure ($^7\text{Be} \rightarrow ^3\text{He} + ^4\text{He}$), the ^3He and ^4He transfer to the target has been suggested as the dominant direct reaction mechanism.

It has been suggested that the two-step ICF could be more likely than a DCT, although a coexistence of the two modes

is not discarded [51,52]. We stay with the above plausible hypothesis that ICF is the main contributor and use the usual definition for total fusion, $\text{TF} = \text{CF} + \text{ICF}$, to report in Table I the total yield of evaporation residues as the total fusion cross section $\sigma_{\text{TF}}^{\text{Exp}}$. It should be stressed, though, that a possible contribution of DCT cannot be discarded from the present measurements.

The elastic scattering experiments of ^{10}B with Al and Si targets [53,54], as well as with a Ni target [55], indicate that the quadrupole deformation and large spin of ^{10}B may have important effects on the corresponding reaction mechanisms. The inclusive character of the present measurements allows us to do only qualitative observations. For the case of the ^{28}Si residue, however, an actual quantitative calculation is made in the next section.

B. Interpretation of proton transfer case in the frame of FRESKO

The experimental cross sections for ^{28}Si production shown in Fig. 4(l) greatly exceed the predictions of the statistical

model calculations, carried out using the PACE2 code. We suggest that some nuclear reaction mechanism other than fusion-evaporation is here involved. The most probable candidate is a direct one-proton transfer to the ^{27}Al target. The Q value for the proton transfer is equal to 5.0 MeV, so it is a very energetically favorable process.

In order to verify this hypothesis, the cross sections $\sigma_{p\text{-tr}}$ for the proton transfer are calculated within the DWBA by using the code FRESKO [56]. Parameters of optical potentials describing $^{10}\text{B} + ^{27}\text{Al}$ and $^9\text{Be} + ^{28}\text{Si}$ interactions in the entrance and exit channels at the corresponding energies are calculated based on the global parametrization presented in Refs. [57,58].

The proton- ^9Be single particle (sp) overlap wave function in ^{10}B , $\phi_{l=1,j=3/2}(r)$, with orbital angular momentum $\ell = 1$ is generated by the interaction potential of Woods-Saxon form with geometric parameters $r_0 = 1.25$ and $a_0 = 0.65$ fm, the sp asymptotic normalization coefficient (ANC) $b = 3.25 \text{ fm}^{-1/2}$, and the spectroscopic factor (SF) $S = 1$ [59].

For each state of ^{28}Si , the Woods-Saxon potentials with the standard geometric parameters $r_0 = 1.25$ and $a_0 = 0.65$ fm, and strengths adjusted to fit the proton binding energy in the given state, are used to generate the normalized (sp) overlap $^{27}\text{Al}(I_a) + p(s_p)$ wave function $\phi_{l_2,j_2}(r)$. This wave function describes the proton motion in the specific state of ^{28}Si (I_f) characterized by the radial quantum number n_r , orbital ℓ_2 , and total angular momenta j_2 , which satisfy the angular-momentum coupling scheme (see, e.g., [60])

$$\begin{aligned} \mathbf{j}_1 &= \mathbf{s}_p + \ell_1, & \mathbf{I}_a &= \mathbf{j}_1 + \mathbf{s}_p, \\ \mathbf{j}_2 &= \mathbf{s}_p + \ell_2, & \mathbf{I}_f &= \mathbf{j}_2 + \mathbf{I}_A, \\ \mathbf{L} &= \mathbf{j}_1 + \mathbf{j}_2 = \ell_1 + \ell_2, \end{aligned} \quad (2)$$

where L is the transferred angular momentum, ℓ_1 , ℓ_2 and j_1 , j_2 are the orbital and total angular momenta of the proton in $^{10}\text{B}(I_a)$ and $^{28}\text{Si}(I_f)$, respectively.

Since the ^{28}Si experimental yield was obtained from the 1.78 MeV γ rays detected, in principle, only states that can populate the 1.78 MeV, 2^+ state in ^{28}Si would need to be considered to compare with the experimental values. However, in order to estimate total $\sigma_{p\text{-tr}}$ cross sections, we took into account transfer reactions to the ground state as well as to the 18 excited states of ^{28}Si , with excitation energies E_x up to 9.5 MeV. This interval of excitation energies includes the so-called Q window [60], where transfer reactions have the maximum yield. The experimental SFs and the reduced widths needed in the calculation were obtained from Ref. [61].

Once the value of $\sigma_{p\text{-tr}}$ was obtained for a given state of ^{28}Si , corresponding branching ratios [62] were applied to estimate the respective contribution to population of the 1.78 MeV, 2^+ state. By adding such contributions from all calculated states, the corrected proton transfer cross sections, $\sigma_{p\text{-tr}}^{\text{corr}}$, are directly compared with the data, as shown in Fig. 5.

The fact that the $\sigma_{p\text{-tr}}^{\text{corr}}$ curve in Fig. 5 agrees very well with the data verifies our hypothesis that the ^{28}Si yield observed in the present experiment originates mainly from proton transfer reactions. One can also conclude that the γ -ray technique used here provides a powerful method to obtain experimentally this

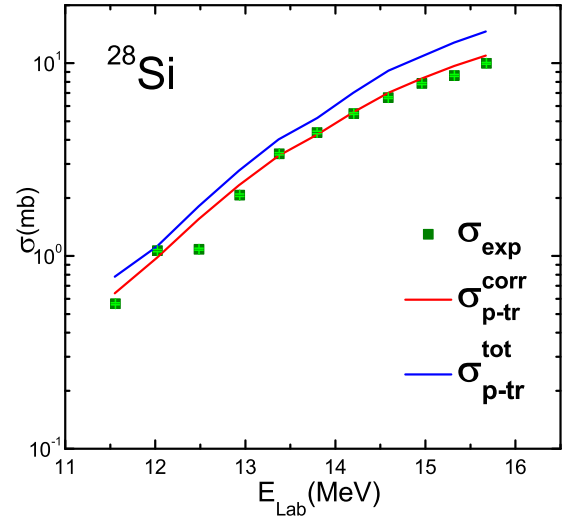


FIG. 5. The measured cross section of ^{28}Si evaporation (squares) in comparison with the proton transfer calculations, $\sigma_{p\text{-tr}}^{\text{corr}}$ (red line). The blue line shows the total proton transfer cross section for the $^{27}\text{Al}(^{10}\text{B}, ^9\text{Be})^{28}\text{Si}$ reaction calculated within the DWBA.

kind of inclusive proton transfer cross sections. “Inclusive” refers in this case to the fact that proton transfers to all states of ^{28}Si that can populate the first excited state, either directly or by subsequent γ decay, are automatically included in the measurement. Along with proper theoretical calculations such as the ones done here with FRESKO, reliable quasiexperimental values for the total proton transfer cross sections, $\sigma_{p\text{-tr}}^{\text{tot}}$, can be obtained.

C. Analysis with CCFULL

In the 1DBPM, the fusion cross section can be calculated from the semiclassical transmission probability [63,64], that mainly depends on the angular momentum and projectile energy imparted from projectile to target nucleus. The method is quite useful to explain fusion at greater energies, but at energies near the barrier the model usually underpredicts the experimental fusion cross section. To elucidate this point, cross sections for the $^{10}\text{B} + ^{27}\text{Al}$ system were calculated using the CCFULL code [65] without inclusion of inelastic excitations. Note that predictions of cross sections from CCFULL code without implementing inelastic channels are considered as 1DBPM. The nucleus-nucleus potential used in the present work is the Akyüz-Winther (A-W) potential [66], where the parameters are $V_0 = 41.83$ MeV, $r_0 = 1.169$ fm, and $a_0 = 0.601$ fm. A comparison of the experimental data and the result obtained from 1DBPM calculations is shown by the black solid line in Fig. 6. As can be seen in the figure, the 1DBPM calculations underpredict the $\sigma_{\text{TF}}^{\text{Exp}}$ substantially, by up to a factor of 3. This strongly suggests that, at the near- and below-barrier energies measured, there is a possible involvement of coupling to intrinsic degrees of freedom.

Thus, coupled channel calculations for different inelastic excitations of the interacting partners without changing the potential parameters were done, and are presented in Fig. 6. The ^{27}Al target provides a suitable deformed nucleus with

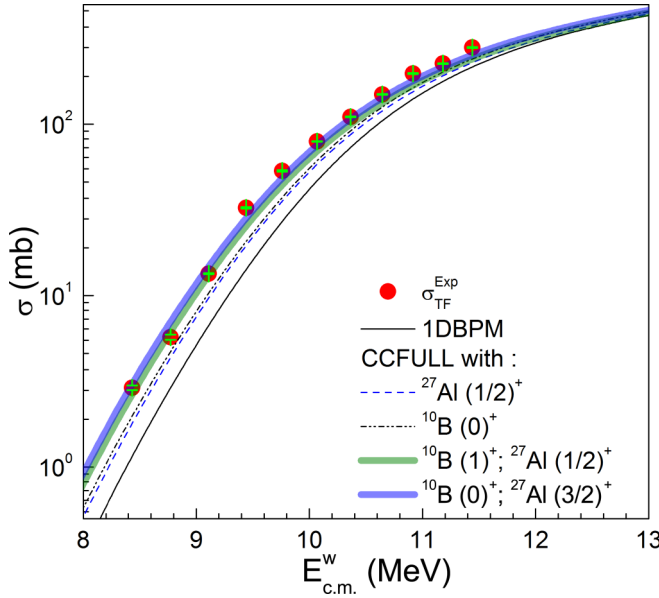


FIG. 6. The experimentally measured excitation function is compared with the 1DBPM, and for different modes of coupling between interacting partners using CCFULL. The inclusion of couplings of different inelastic excitations of interacting partners is shown. Lines and curves are self-explanatory. Symbols represent experimental total fusion cross section \pm SE.

a nonzero spin, i.e., $5/2^+$ ground state, which can be a reason for the enhancement in the experimental cross sections. Therefore, keeping the projectile as inert, we started with the inclusion of the well resolved first excited state at 0.84 MeV ($1/2^+$) with one-phonon coupling and placing the value of deformation $\beta \approx -0.392$ in the input card of the CCFULL code. As can be seen in Fig. 6, the coupled channel calculation (blue dashed line) enhances the fusion cross section as compared to the 1DBPM calculations but still underpredicts the $\sigma_{\text{TF}}^{\text{Exp}}$. A further inclusion of the second excited state of ^{27}Al at 1.014 MeV ($3/2^+$) with two-phonon coupling (not shown) slightly enhances the sub-barrier fusion cross section when compared to the previous values. In a similar way, keeping target as inert and including the first excited state of projectile (^{10}B) at 0.718 MeV (1^+), considering the deformation parameter $\beta \approx -0.55$ [67], gives a fusion cross section that still is not satisfactory, as in the previous coupling attempts. Considering in addition the second excited state of the projectile at 1.740 MeV (0^+) including two-phonon coupling, the fusion cross section (black dash-dot-dot line) is found to be slightly improved. On comparing the first four coupling calculations, it can be inferred that the coupling to inelastic channels of the projectile yields higher enhancement than the similar coupling relative to the target. But still the coupling calculations are found to be lower than the experimental data $\sigma_{\text{TF}}^{\text{Exp}}$.

Related to previous coupling calculations, the intermediate combinations were also attempted to deduce total fusion cross sections from the CCFULL code. For an example, considering single-phonon coupling with the first excited state of ^{10}B and ^{27}Al gives an improved version of fusion cross section (solid

green band) with respect to previous calculated values. However, inclusion of the first two excited states of both ^{10}B and ^{27}Al together, with up to two phonon couplings, enhances the sub-barrier fusion cross sections (blue solid band) thus fairly reproducing the $\sigma_{\text{TF}}^{\text{Exp}}$ in the studied energy range. The purpose of presenting the green and blue bands is to emphasize that $\sigma_{\text{TF}}^{\text{Exp}}$ follows intermediate coupling over the entire range of studied energies. This indicates that coupling calculations are important to describe the total fusion cross section without any modification in the ion-ion potential parameters for the $^{10}\text{B} + ^{27}\text{Al}$ system.

D. Interpretation of $\sigma_{\text{TF}}^{\text{Exp}}$ in frame of astrophysical S factor and $L(E)$ factor

The astrophysical S factor is an important parameter to define the hindrance effect that has been observed in medium and heavy systems where the fusion Q value is always positive [68]. Since the $^{10}\text{B} + ^{27}\text{Al}$ system has a positive Q value of 25.8 MeV, an attempt has been made to interpret the experimental data in the frame of the astrophysical S factor. It is important to mention that several experiments were attempted recently to search for the possible existence of the hindrance effect [69–71] from the S factor measurements. This is because of the fact that fusion reactions of light systems are relevant to interstellar evolution, and the accurate knowledge of sub-barrier fusion cross sections is essential for the validation of nucleosynthesis simulations.

The astrophysical S factor is defined as

$$S(E_{\text{c.m.}}) = E_{\text{c.m.}} \sigma(E_{\text{c.m.}}) \exp(2\pi\eta), \quad (3)$$

where η is the Sommerfeld parameter ($Z_1 Z_2 e^2 / \hbar v$, and v is the beam velocity), $\sigma(E_{\text{c.m.}})$ is the fusion cross section, and $E_{\text{c.m.}}$ is the projectile energy in the center-of-mass frame. Using Eq. (3), the astrophysical S factor values are extracted from $\sigma_{\text{TF}}^{\text{Exp}}$ and are compared with the theoretical predictions (i.e., 1DBPM and coupled-channel) in Fig. 7. As can be seen in the figure, the S factor experimental values do not exhibit a maximum and are continuously increasing with decreasing energy for the entire sub-barrier energy range, following the coupled-channel calculations. This indicates the absence of saturation of the S factor within the measured energy range, thus no fusion hindrance can be claimed for the $^{10}\text{B} + ^{27}\text{Al}$ system. In order to have a clearer picture about the possible appearance of fusion hindrance in the sub-barrier region, many nuclear physicists considered a reliable $L(E_{\text{c.m.}})$ factor approach. This factor is defined as the logarithmic slope of the excitation functions and can be calculated as

$$L(E_{\text{c.m.}}) = \frac{d[\ln(E_{\text{c.m.}} \sigma)]}{dE_{\text{c.m.}}}. \quad (4)$$

Using Eq. (4), the experimental and theoretical logarithmic slopes of fusion excitation functions are deduced considering the point difference method of differentiation and keeping the same interval between the data points. As can be seen in the inset of Fig. 7, there is no pronounced change of slope $L(E_{\text{c.m.}})$ in the below-barrier region and the mean trend keeps rising towards the lowest measured energy. The black dotted line represents the L_{CS} line, which shows that when $L(E_{\text{c.m.}})$ equals $\pi\eta/E_{\text{c.m.}}$ the system can be taken to be at the threshold for

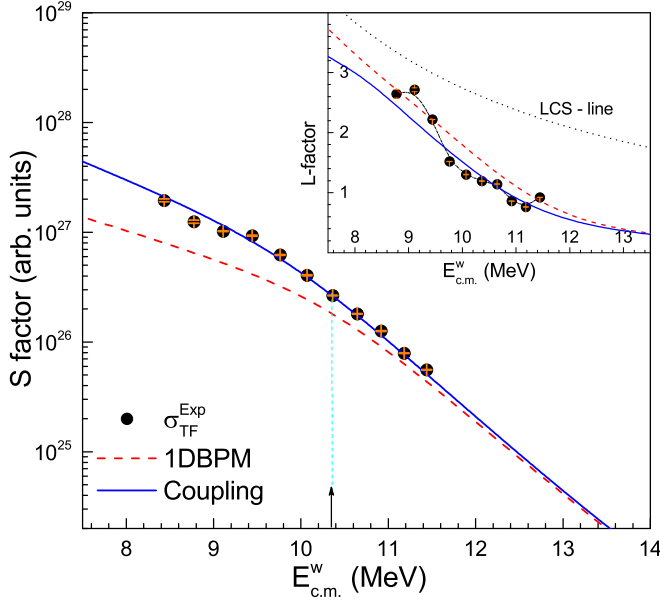


FIG. 7. Astrophysical S factor derived from experimental total fusion cross sections in the $^{10}\text{B} + ^{27}\text{Al}$ system. In the inset, the logarithmic derivative $L(E)$ factor is plotted as a function of the center-of-mass energy. The lines and curves are self-explanatory. Symbols represents experimental total fusion cross section \pm SE.

fusion hindrance [72–75]. At the studied energies there is no crossover observed between the L_{CS} and $L(E_{c.m.})$ and both are significantly separated from each other. This suggests that the $^{10}\text{B} + ^{27}\text{Al}$ system can be considered as a soft system [72–76], where no threshold of fusion hindrance occurs till $\approx 20\%$ below the barrier. It will be interesting to extend this work at deep sub-barrier energies where the total fusion cross section is down to $1 \mu\text{b}$. In this region there might be possible chances of getting fusion hindrance by measuring a new experimental total fusion cross section; however, extrapolating conventional coupled channel calculations suggests the absence of fusion hindrance.

E. Interpretation of data in the frame of UFF

To study the systematic behavior of $\sigma_{\text{TF}}^{\text{Exp}}$ for the $^{10}\text{B} + ^{27}\text{Al}$ system together with total fusion experimental data for other light systems [34,36–41], a reliable reduction technique—which eliminates geometrical effects without taking into account the coupling effects through inelastic or breakup channels as described in Ref. [77]—is adopted. In this technique, the experimental fusion cross section and projectile energy are reduced to dimensionless quantities as

$$\sigma_{\text{red}} \text{ or } F_{\text{TF}}^{\text{Exp}}(x) = \frac{2 E_{c.m.} \sigma_{\text{TF}}^{\text{Exp}}}{R_b^2 \hbar \omega}, \quad (5)$$

$$E_{\text{red}} \text{ or } x = \frac{E_{c.m.} - V_b}{\hbar \omega}, \quad (6)$$

where R_b , V_b , and $\hbar \omega$ are the barrier radius, barrier height, and barrier curvature, respectively. To have a consistent comparison with other light systems, viz., $^7\text{Li} + ^{24}\text{Mg}$ [34], $^6\text{Li} + ^{24}\text{Mg}$ [34], $^7\text{Li} + ^{27}\text{Al}$ [36], $^9\text{Be} + ^{27}\text{Al}$ [38,39],

TABLE II. Uncoupled barrier parameters calculated from A-W potentials for several systems.

System	R_b (fm)	V_b (MeV)	$\hbar \omega$ (MeV)
$^7\text{Li} + ^{24}\text{Mg}$	8.17	5.89	2.91
$^6\text{Li} + ^{24}\text{Mg}$	8.04	5.97	3.14
$^7\text{Li} + ^{27}\text{Al}$	8.29	6.29	2.94
$^9\text{Be} + ^{27}\text{Al}$	8.41	8.27	3.01
$^{19}\text{F} + ^{19}\text{F}$	8.56	12.64	3.04
$^{18}\text{O} + ^{27}\text{Al}$	8.83	15.75	3.11
$^{17}\text{O} + ^{27}\text{Al}$	8.75	15.88	3.19
$^{16}\text{O} + ^{27}\text{Al}$	8.66	16.03	3.28
$^{10}\text{B} + ^{27}\text{Al}^a$	8.36	10.38	3.22

^aPresent work.

$^{19}\text{F} + ^{19}\text{F}$ [40], $^{18}\text{O} + ^{27}\text{Al}$ [41], $^{17}\text{O} + ^{27}\text{Al}$ [41], and $^{16}\text{O} + ^{27}\text{Al}$ [41] in the frame of above discussed equations, we calculated the static quantities R_b , V_b , and $\hbar \omega$ using the A-W ion-ion potential predictions. These static quantities, tabulated in Table II, are well related to the Wong’s cross sectional formula σ_{Wong} [78]; therefore, by using σ_{Wong} instead of $\sigma_{\text{TF}}^{\text{Exp}}$, Eq. (5) can be reduced to a fusion function (i.e., $F_{\text{UFF}} = \ln[1 + \exp(2\pi x)]$) which is universally equal for all projectile-target combinations; for this reason it is called the universal fusion function (UFF) [77].

Thus, UFF is a benchmark curve which does not consider any coupling quantities at sub-barrier energies and is a possible way to understand the influence of breakup or other coupling effects on fusion cross sections. Recently, Aversa *et al.* [35] transformed the traditional experimental fusion function [Eq. (5)] by introducing a correction factor, i.e., $\sigma_{\text{Wong}}/\sigma_{1\text{DBPM}}$, and utilized the modified experimental fusion function to compare several systems involving the heavy nucleus ^{197}Au . The authors claimed that enhancement associated with the ^{10}B projectile is due to the coupling to one neutron pickup transfer when compared to other projectiles (^6Li , ^7Li , ^9Be).

To understand the behavior of total fusion cross sections in lighter systems we adopted the similar approach as given in Ref. [35]. The experimental fusion function is deduced for the aforesaid lighter systems and the results are compared with the standard UFF in Fig. 8. As can be seen in the figure, $^7\text{Li} + ^{24}\text{Mg}$ [34], $^6\text{Li} + ^{24}\text{Mg}$ [34], and $^{10}\text{B} + ^{27}\text{Al}$ (present work) are the only lighter systems that have experimental data points in sub- and near-barrier energies, whereas the rest of systems were measured only at energies near and above the Coulomb barrier. A comparison of $^7\text{Li} + ^{24}\text{Mg}$ [34], $^6\text{Li} + ^{24}\text{Mg}$ [34], and $^{10}\text{B} + ^{27}\text{Al}$ (present work) with UFF at below-barrier energies shows slight enhancements that reveal the importance of inelastic excitations of projectile and/or target to explain the total fusion cross section. For other lighter systems, at energies near and above barrier, the reduced total fusion cross section is found to nearly follow the UFF curve, suggesting no interplay of coupling effects on fusion data.

However, for the $^7\text{Li} + ^{24}\text{Mg}$ [35] and $^6\text{Li} + ^{24}\text{Mg}$ [35] systems, at above-barrier energies, the reduced total fusion cross section is found to be slightly suppressed, which may be because of significant contribution from the coupling to

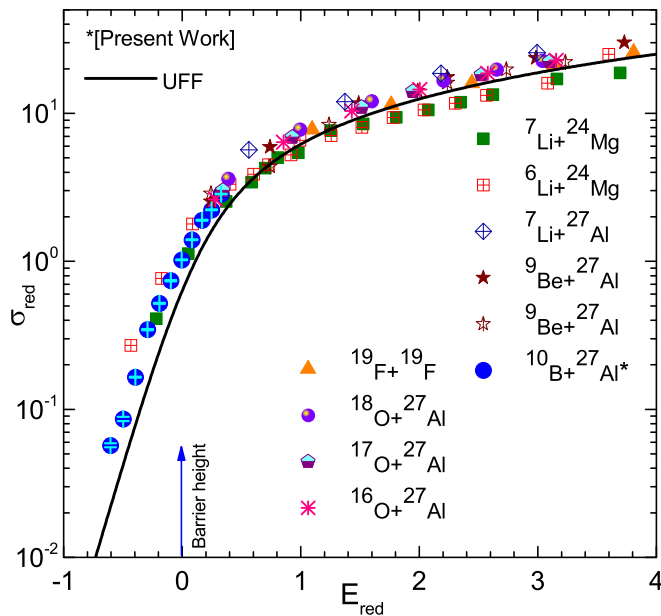


FIG. 8. Reduced total fusion cross section as a function of the reduced energy for several nuclear systems. The solid line represent the UFF. The arrow at $E_{red} = 0$ corresponds to the barrier height.

breakup channels [26]. It is important to mention that there are no available experimental total fusion data at sub- and near-barrier energies for enough systems to make a reliable systematic study, therefore, it is important to measure σ_{TF}^{Exp} for other projectile-target combinations at below-barrier energies for the justification of any systematics in the frame of the UFF curve. Nevertheless it would be interesting to perform CCFULL calculations including inelastic couplings for the two additional systems with a few points below the barrier in Fig. 8, i.e., $^{6,7}\text{Li} + ^{24}\text{Mg}$, which could help to confirm the present findings about the observed fusion enhancement in the sub-barrier region.

IV. SUMMARY AND CONCLUSIONS

In this work we have measured the cross sections for the characteristic γ rays of the residual nuclei resulting from

reactions of the $^{10}\text{B} + ^{27}\text{Al}$ system between ≈ 2.6 MeV below and ≈ 1.5 MeV above the Coulomb barrier. The cross sections for different evaporation channels as well as the total fusion cross sections were deduced and analyzed in the frame of several models.

The 1DBPM fails to reproduce the total fusion cross sections at the studied energies. ICF and/or direct cluster transfer are suggested as possible mechanisms contributing to the observed discrepancies with the statistical model results, but the ICF hypothesis is assumed. DWBA calculations strongly suggest the formation of ^{28}Si via the one-proton transfer reaction and confirm in turn the power of the γ -ray technique to make inclusive transfer measurements.

The total fusion cross sections are, however, found to be in good agreement with results obtained from the coupled channel code CCFULL at such energies, where the standard Akyüz-Winther potential parameters were used. The enhancement observed in the total fusion cross sections was thus explained by the inclusion of inelastic couplings associated with both target and projectile.

From the analysis of the astrophysical S factor as well as the $L(E_{c.m.})$ factor, it was observed that 1DBPM starts to saturate at near-barrier energies whereas coupled channel calculations, which follow the experimental data, do not attain a maximum even at $\approx 20\%$ below the barrier.

A comparative study has been attempted in the frame of the UFF, which reveals that the enhancement observed in the sub-barrier energy region for the present system seems to appear also in other similar systems, but there are not enough measurements in this energy region to draw final conclusions.

ACKNOWLEDGMENTS

The authors acknowledge the technician Pedro Villaseñor for keeping the accelerator running during the experiment. E.F.A. and V.R.S. thank the CONACyT for providing financial support under Project No. CB-01-254619. L.A. and V.R.S. thank the CONACyT-314857 and DGAPA-UNAM IN 107820 for financial support. T.L.B. thanks UAEMex for providing financial support under Project No. 6258/2020CIB.

-
- [1] E. F. Aguilera, P. Amador-Valenzuela, E. Martinez-Quiroz, J. Fernandez-Arnaiz, J. J. Kolata, and V. Guimaraes, *Phys. Rev. C* **93**, 034613 (2016).
- [2] M. Dasgupta, D. J. Hinde, R. D. Butt, R. M. Anjos, A. C. Berriman, N. Carlin, P. R. S. Gomes, C. R. Morton, J. O. Newton, A. Szantode Toledo, and K. Hagino, *Phys. Rev. Lett.* **82**, 1395 (1999).
- [3] F. D. Becchetti and J. J. Kolata (TwinSol Collaboration), *Nucl. Instrum. Methods Phys. Res., Sect. B*, **376**, 397 (2016).
- [4] A. Yadav, P. P. Singh, M. Shuaib, V. R. Sharma, I. Bala, Unnati, S. Gupta, D. P. Singh, M. K. Sharma, R. Kumar, S. Murlithar, R. P. Singh, B. P. Singh, and R. Prasad, *Phys. Rev. C* **96**, 044614 (2017).
- [5] V. R. Sharma, A. Yadav, P. P. Singh, D. P. Singh, S. Gupta, M. K. Sharma, I. Bala, R. Kumar, S. Murlithar, B. P. Singh, and R. Prasad, *Phys. Rev. C* **89**, 024608 (2014).
- [6] J. J. Kolata *et al.*, *Eur. Phys. J. A* **52**, 123 (2016), and the references therein.
- [7] B. Mukeru, G. J. Rampho, and M. L. Lekala, *J. Phys. G: Nucl. Part. Phys.* **45**, 045101 (2018).
- [8] A. Kumari and R. Kharab, *Nucl. Phys. A* **941**, 38 (2015).
- [9] V. Morcelle *et al.*, *Phys. Lett. B* **732**, 228 (2014).
- [10] A. Pakou *et al.*, *Eur. Phys. J. A* **51**, 90 (2015).
- [11] A. Pakou, L. Acosta, P. D. OMalley, S. Aguilar, E. F. Aguilera, M. Baines, D. Bardayan, F. D. Becchetti, C. Boomershine, M. Brodeur, F. Cappuzzello, S. Carmichael, L. Caves, E. Chavez,

- C. Flores-Vazquez, A. Gula, J. J. Kolata, B. Liu, D. J. Marin-Lambarri, F. F. Morales, K. Rusek, A. M. Sanchez-Benitez, O. Sgouros, V. R. Sharma, V. Soukeras, and G. Souliotis, *Phys. Rev. C* **102**, 031601(R) (2020).
- [12] Md. Moin Shaikh *et al.*, *Phys. Rev. C* **90**, 024615 (2014).
- [13] A. Shrivastava *et al.*, *Phys. Lett. B* **755**, 332 (2016).
- [14] R. N. Sahoo, M. Kaushik, A. Sood, P. Kumar, A. Sharma, S. Thakur, P. P. Singh, P. K. Raina, M. M. Shaikh, R. Biswas, A. Yadav, J. Gehlot, S. Nath, N. Madhavan, V. Srivastava, M. K. Sharma, B. P. Singh, R. Prasad, A. Rani, A. Banerjee, U. Gupta, N. K. Deb, and B. J. Roy, *Phys. Rev. C* **99**, 024607 (2019).
- [15] E. Martinez-Quiroz *et al.*, *Phys. Rev. C* **90**, 014616 (2014).
- [16] D. J. Hinde, M. Dasgupta, B. R. Fulton, C. R. Morton, R. J. Wooliscroft, A. C. Berriman, and K. Hagino, *Phys. Rev. Lett.* **89**, 272701 (2002).
- [17] M. Dasgupta, P. R. S. Gomes, D. J. Hinde, S. B. Moraes, R. M. Anjos, A. C. Berriman, R. D. Butt, N. Carlin, J. Lubian, C. R. Morton, J. Newton, and A. Szantode Toledo, *Phys. Rev. C* **70**, 024606 (2004).
- [18] C. S. Palshetkar, S. Thakur, V. Nanal, A. Shrivastava, N. Dokania, V. Singh, V. V. Parkar, P. C. Rout, R. Palit, R. G. Pillay, S. Bhattacharyya, A. Chatterjee, S. Santra, K. Ramachandran, and N. L. Singh, *Phys. Rev. C* **89**, 024607 (2014).
- [19] A. Mukherjee *et al.*, *Phys. Lett. B* **91**, 636 (2006).
- [20] Md. Moin Shaikh *et al.*, *J. Phys. G: Nucl. Part. Phys.* **45**, 095103 (2018).
- [21] A. Sood *et al.*, *J. Phys. G: Nucl. Part. Phys.* **48**, 025105 (2020).
- [22] V. R. Sharma *et al.*, *J. Phys. G: Nucl. Part. Phys.* **45**, 056113 (2015).
- [23] V. R. Sharma *et al.*, *Nucl. Phys. A* **946**, 182193 (2016).
- [24] I. Lee and A. Diaz-Torres, *J. Phys. G* **47**, 015101 (2020).
- [25] L. F. Canto, P. R. S. Gomes, R. Donangelo, J. Lubian, and M. S. Hussein, *Phys. Rep.* **596**, 1 (2015).
- [26] H. Kumawat, V. Jha, V. V. Parkar, B. J. Roy, S. K. Pandit, R. Palit, P. K. Rath, C. S. Palshetkar, S. K. Sharma, S. Thakur, A. K. Mohanty, A. Chatterjee, and S. Kailas, *Phys. Rev. C* **86**, 024607 (2012).
- [27] C. Beck, F. A. Souza, N. Rowley, S. J. Sanders, N. Aissaoui, E. E. Alonso, P. Bednarczyk, N. Carlin, S. Courtin, A. Diaz-Torres, A. Dummer, F. Haas, A. Hachem, K. Hagino, F. Hoellinger, R. V. F. Janssens, N. Kintz, R. LiguoriNeto, E. Martin, M. M. Moura, M. G. Munhoz, P. Papka, M. Rousseau, A. Sanchez Zafra, O. Stezowski, A. A. Suaide, E. M. Szanto, A. Szantode Toledo, S. Szilner, and J. Takahashi, *Phys. Rev. C* **67**, 054602 (2003).
- [28] A. DiPietro, P. Figuera, E. Strano, M. Fisichella, O. Goryunov, M. Lattuada, C. Maiolino, C. Marchetta, M. Milin, A. Musumarra, V. Ostashko, M. G. Pellegriti, V. Privitera, G. Randisi, L. Romano, D. Santonocito, V. Scuderi, D. Torresi, and M. Zadro, *Phys. Rev. C* **87**, 064614 (2013).
- [29] H. M. Jia, C. J. Lin, L. Yang, X. X. Xu, N. R. Ma, L. J. Sun, F. Yang, Z. D. Wu, H. Q. Zhang, Z. H. Liu, and D. X. Wang, *Phys. Lett. B* **43**, 755 (2016).
- [30] V. V. Sargsyan, G. Scamps, G. G. Adamian, N. V. Antonenko, and D. Lacroix, *Phys. Rev. C* **88**, 064601 (2013).
- [31] Z. Kohley, J. F. Liang, D. Shapira, R. L. Varner, C. J. Gross, J. M. Allmond, A. L. Caraley, E. A. Coello, F. Favela, K. Lagergren, and P. E. Mueller, *Phys. Rev. Lett.* **107**, 202701 (2011).
- [32] P. Jacobs, Z. Fraenkel, G. Mamane *et al.*, *Phys. Lett. B* **175**:3, 271 (1986).
- [33] C. J. Lin *et al.*, *EPJ Web Conf.* **66**, 03055 (2014).
- [34] M. Ray, A. Mukherjee, M. K. Pradhan, R. Kshetri, M. S. Sarkar, R. Palit, I. Majumdar, P. K. Joshi, H. C. Jain, and B. Dasmahapatra, *Phys. Rev. C* **78**, 064617 (2008).
- [35] M. Aversa, D. Abriola, M. A. G. Alvarez, A. Arazi, M. A. Cardona, L. C. Chamon, E. deBarbara, J. deJesus, J. P. Fernandez-Garcia, L. R. Gasques, D. Hojman, A. Lepine-Szily, G. V. Marti, A. J. Pacheco, V. Scarduelli, and V. A. B. Zagatto, *Phys. Rev. C* **101**, 044601 (2020).
- [36] K. Kalita, S. Verma, R. Singh, J. J. Das, A. Jhingan, N. Madhavan, S. Nath, T. Varughese, P. Sugathan, V. V. Parkar, K. Mahata, K. Ramachandran, A. Shrivastava, A. Chatterjee, S. Kailas, S. Barua, P. Basu, H. Majumdar, M. Sinha, R. Bhattacharya, and A. K. Sinha, *Phys. Rev. C* **73**, 024609 (2006).
- [37] J. R. Maiorino *et al.*, *Braz. J. Phys.* **34**, 3A (2004).
- [38] G. V. Marti, P. R. S. Gomes, M. D. Rodriguez, J. O. FernandezNiello, O. A. Capurro, A. J. Pacheco, J. E. Testoni, M. Ramirez, A. Arazi, I. Padron, R. M. Anjos, J. Lubian, and E. Crema, *Phys. Rev. C* **71**, 027602 (2005).
- [39] R. M. Anjos *et al.*, *Phys. Lett. B* **534**, 45 (2002).
- [40] R. M. Anjos, V. Guimaraes, N. Added, N. CarlinFilho, M. M. Coimbra, L. Fante, M. C. S. Figueira, E. M. Szanto, C. F. Tenreiro, and A. Szantode Toledo, *Phys. Rev. C* **42**, 354 (1990).
- [41] Y. Eisen *et al.*, *Nucl. Phys. A* **291**, 459 (1977).
- [42] E. F. Aguilera, Ph.D. Thesis, Department of Physics, University of Notre Dame, 1985 (unpublished).
- [43] E. F. Aguilera, *Rev. Mex. Fis.* **43** (Suppl.1), 130 (1997).
- [44] *Table of Isotopes*, 8th ed., edited by R. B. Firestone and V. S. Shirley (Wiley, New York, 1996).
- [45] E. F. Aguilera, J. J. Vega, J. J. Kolata, A. Morsad, R. G. Tighe, and X. J. Kong, *Phys. Rev. C* **41**, 910 (1990).
- [46] A. Gavron, *Phys. Rev. C* **21**, 230 (1980).
- [47] M. Wang *et al.*, *Chin. Phys. C* **36**(12), 1603 (2012).
- [48] R. G. Stokstad, in *Treatise on Heavy Ion Science*, edited by D. A. Bromley (Plenum, New York, 1985), Vol. 3, p. 94.
- [49] N. Carlin Filho, M. M. Coimbra, N. Added, R. M. dos Anjos, L. Fante, Jr., M. C. S. Figueira, V. Guimaraes, E. M. Szanto, A. Szanto de Toledo, and O. Civitarese, *Phys. Rev. C* **40**, 91 (1989).
- [50] O. Sgouros, A. Pakou, D. Pierroutsakou, M. Mazzocco, L. Acosta, X. Aslanoglou, C. Betsou, A. Boiano, C. Boiano, D. Carbone, M. Cavallaro, J. Grebosz, N. Keeley, M. LaCommara, C. Manea, G. Marquinez-Duran, I. Martel, N. G. Nicolis, C. Parascandolo, K. Rusek, A. M. Sanchez-Benitez, C. Signorini, F. Soramel, V. Soukeras, C. Stefanini, E. Stiliaris, E. Strano, I. Strojek, and D. Torresi, *Phys. Rev. C* **94**, 044623 (2016).
- [51] M. Sinha *et al.*, *Eur. Phys. J. A* **44**, 403 (2010).
- [52] F. A. Souza *et al.*, *Nucl. Phys. A* **821**, 36 (2009).
- [53] L. A. Parks, K. W. Kemper, A. H. Lumpkin, R. I. Cutler *et al.*, *Phys. Lett. B* **70**, 27 (1977).
- [54] L. A. Parks, K. W. Kemper, R. I. Cutler and L. H. Harwood, *Phys. Rev. C* **19**, 2206 (1979).
- [55] V. Scarduelli, E. Crema, V. Guimaraes, D. Abriola, A. Arazi, E. deBarbara, O. A. Capurro, M. A. Cardona, J. Gallardo, D. Hojman, G. V. Marti, A. J. Pacheco, D. Rodrigues, Y. Y. Yang, N. N. Deshmukh, B. Paes, J. Lubian, D. R. MendesJunior, V. Morcelle, and D. S. Monteiro, *Phys. Rev. C* **96**, 054610 (2017).
- [56] I. J. Thompson, *Comput. Phys. Rep.* **7**, 167 (1988).
- [57] Y. Xu, Y. Han, H. Liang, Z. Wu, H. Guo, and C. Cai, *Phys. Rev. C* **99**, 034618 (2019).

- [58] Y. Xu, Y. Han, H. Liang, Z. Wu, H. Guo, and C. Cai, *Chin. Phys. C* **44**, 034101 (2020).
- [59] J. T. Huanga, C. A. Bertulani, and V. Guimaraes, *At. Data Nucl. Data Tables* **96**, 824 (2010).
- [60] G. R. Satchler, *Direct Nuclear Reactions* (Clarendon, Oxford, 1983).
- [61] B. J. Cole, A. Watt, and R. R. Whitehead, *J. Phys. G: Nucl. Phys.* **2**, 501 (1976).
- [62] M. Shamsuzzoha Basunia, *Nucl. Data Sheets* **114**, 1189 (2013).
- [63] K. Hagino and A. B. Balantekin, *Phys. Rev. A* **70**, 032106 (2004).
- [64] N. Takigawa, T. Masamoto, T. Takehi, and T. Rumin, *J. Korean Phys. Soc. Suppl.* **43**, S91 (2003).
- [65] K. Hagino, N. Rowley, and T. Kruppa, *Comput. Phys. Commun.* **123**, 143 (1999).
- [66] Ö. Akyüz and A. Winther, in *Proceedings of the Enrico Fermi School of Physics, 1979, Course on Nuclear Structure and Heavy-ion Reactions*, edited by R. A. Broglia, C. H. Dasso, and R. Ricci (North Holland, Amsterdam, 1981).
- [67] L. I. Galanina *et al.*, *Phys. At. Nucl.* **68**, 1957 (2005).
- [68] G. Montagnoli, A. M. Stefanini, C. L. Jiang, K. Hagino, F. Galtarossa, G. Colucci, S. Bottoni, C. Brogini, A. Caciolli, P. Colovic, L. Corradi, S. Courtin, R. Depalo, E. Fioretto, G. Fruet, A. Gal, A. Goasduff, M. Heine, S. P. Hu, M. Kaur, T. Mijatovic, M. Mazzocco, D. Montanari, F. Scarlassara, E. Strano, S. Szilner, and G. X. Zhang, *Phys. Rev. C* **97**, 024610 (2018).
- [69] B. B. Back, H. Esbensen, C. L. Jiang, and K. E. Rehm, *Rev. Mod. Phys.* **86**, 317 (2014).
- [70] G. Montagnoli and A. M. Stefanini, *Eur. Phys. J. A* **53**, 169 (2017).
- [71] T. Ichikawa, K. Hagino, and A. Iwamoto, *Phys. Rev. C* **75**, 057603 (2007).
- [72] C. L. Jiang, K. E. Rehm, B. B. Back, and R. V. F. Janssens, *Phys. Rev. C* **75**, 015803 (2007).
- [73] C. L. Jiang, H. Esbensen, K. E. Rehm, B. B. Back, R. V. F. Janssens, J. A. Caggiano, P. Collon, J. Greene, A. M. Heinz, D. J. Henderson, I. Nishinaka, T. O. Pennington, and D. Seweryniak, *Phys. Rev. Lett.* **89**, 052701 (2002); C. L. Jiang *et al.*, *Phys. Rev. C* **71**, 044613 (2005); *Phys. Lett. B* **640**, 18 (2006); *Phys. Rev. Lett.* **113**, 022701 (2014).
- [74] C. L. Jiang, B. B. Back, H. Esbensen, R. V. F. Janssens, and K. E. Rehm, *Phys. Rev. C* **73**, 014613 (2006).
- [75] C. L. Jiang, K. E. Rehm, R. V. F. Janssens, H. Esbensen, I. Ahmad, B. B. Back, P. Collon, C. N. Davids, J. P. Greene, D. J. Henderson, G. Mukherjee, R. C. Pardo, M. Paul, T. O. Pennington, D. Seweryniak, S. Sinha, and Z. Zhou, *Phys. Rev. Lett.* **93**, 012701 (2004).
- [76] C. L. Jiang, H. Esbensen, B. B. Back, R. V. F. Janssens, and K. E. Rehm, *Phys. Rev. C* **69**, 014604 (2004).
- [77] L. F. Canto *et al.*, *Nucl. Phys. A* **821(51)**, 9671 (2009).
- [78] C. Y. Wong, *Phys. Rev. Lett.* **31**, 766 (1973).